SUPPLEMENTARY INFORMATION

Ultraviolet Photoeffects on Oxygen-Hydrogen Interstitial Clusters in Rutile TiO_2

Heonjae Jeong[b,c], Ian I. Suni[a], Raylin Chen[a], Grace McKnight[b], Elif Ertekin[b], Xiao Su[a] and Edmund G. Seebauer[a]*

[a] Department of Chemical and Biomolecular Engineering, University of Illinois at Urbana-Champaign, Urbana, Illinois 61801, United States

[b] Department of Mechanical Science and Engineering, University of Illinois at Urbana-Champaign, Urbana, Illinois 61801, United States

[c] Current address: Department of Mechanical Engineering, Sogang University, Seoul 04107, South Korea

* Corresponding author, eseebaue@illinois.edu

1. Method for determination of profile metrics

Determination of the profile metrics F_{18}, λ_1 and λ_2 has been detailed elsewhere[1] and will be only summarized here. Decay of the ^{18}O concentration beyond the peak obeyed a bi-exponential functional form having two widely separated decay constants, $\lambda_1 << \lambda_2$. Decay according to λ_1 dominated the change in ^{18}O concentration near the peak and reached a plateau typically 3-10% above the natural abundance of ^{18}O (C_O =1.276 × 10^{20} cm^{-3}) in TiO_2. This plateau signified the beginning of decay according to λ_2.

In each profile, the concentration characterizing this plateau was normalized with respect to C_O to yield a dimensionless scaling factor Z, which typically varied from 1.03 to 1.1. The functional form phenomenologically describing the λ_1 region was:

$$C(x) = C_O\left[\frac{C_{OT} - C_O}{C_o} e^{-\frac{x}{\lambda_1} + b_1} + Z\right] \qquad \text{(S1)},$$

where *C(x)* denotes the concentration of ^{18}O at a depth *x* below the surface, C_{OT} is the total concentration of O atoms in the TiO_2 lattice (6.38 × 10^{22} cm^{-3}), and b_1 is a phenomenological amplitude factor. A similar expression described decay of *C(x)* in the λ_2 region down to Z=1:

$$C(x) = C_O\left[\frac{C_{OT} - C_O}{C_O} e^{-\frac{x}{\lambda_2} + b_2} + 1\right] \quad \text{(S2)},$$

where b_2 is a second phenomenological amplitude factor.

Eq. (S1) was fit to the λ_1 region of the profile using a nonlinear least squares algorithm to determine λ_1, b_2 and Z. The range of depths contributing to the fit typically lay between x=α, which is near the peak, and α+4λ_1.

SIMS measurements stopped at depths much shallower than λ_2. However, with α, λ_1, b_1, and Z known, λ_2 and b_2 could be determined mathematically by requiring continuity at the boundary between the λ_1 and λ_2 regions of both the profile itself and its first derivative. We consistently set this boundary at a depth equal to α+4λ_1. Requiring continuity of the profile itself at α+4λ_1 means setting Eq. (S1) equal to Eq. (S2) at x = α+4λ_1 to yield

$$ln\left[e^{\frac{-\alpha - 4\lambda_1}{\lambda_1} + b_1} + \frac{C_O(Z-1)}{(C_{OT} - C_O)}\right] = \frac{-\alpha - 4\lambda_1}{\lambda_2} + b_2 \quad \text{(S3)}.$$

Requiring continuity of the first derivative yields

$$\frac{1}{\lambda_1} e^{-\frac{x}{\lambda_1} + b_1} = \frac{1}{\lambda_2} e^{-\frac{x}{\lambda_2} + b_2} \quad \text{(S4)}.$$

Simultaneous solution of Eqs. (S3) and (S4) yields

$$\lambda_2 = \lambda_1\left[1 + \frac{C_O(Z-1)}{(C_{OT} - C_O)} e^{\frac{\alpha}{\lambda_1} + 4 - b_1}\right] \quad \text{(S5)}.$$

Substitution of this value of λ_2 back into either Eq. (S3) or (S4) yields b_2.

The net flux F_{18} was computed as

$$F_{18} = N_{18}/t \quad \text{(S6)},$$

where N_{18} denotes the number of injected ^{18}O atoms. N_{18} was computed as the integral of (C-C_O) throughout the entire solid. This integral was performed piecewise. The number N_{VP} of injected ^{18}O atoms appearing in the valley-peak region between x = 0 and α was obtained by numerical trapezoidal-rule integration of (C-C_O). For x > α, contributions to the integral from the λ_1 and λ_2 regions of the profile were computed analytically using Eq. (S1) and (S2) for C together with the

parameters λ_1, λ_2, Z, b_1 and b_2 determined as described above. The number of atoms in the λ_1 region, $N_{\lambda 1}$, is

$$N_{\lambda 1} = \int_{\alpha}^{\alpha + 4\lambda 1} \left[C_O \left[\frac{C_{OT} - C_O}{C_O} \left(e^{-\frac{x}{\lambda_1} + b_1} \right) + Z \right] - C_O \right] dx \quad \text{(S7)},$$

while the corresponding number $N_{\lambda 2}$ in the λ_2 region is

$$N_{\lambda 2} = \int_{\alpha + 4\lambda_1}^{\infty} \left[C_O \left[\frac{C_{OT} - C_O}{C_O} \left(e^{-\frac{x}{\lambda_2} + b_2} \right) + 1 \right] - C_O \right] dx \quad \text{(S8)}.$$

Performing the analytical integration and adding all the piecewise components together yields:

$$N_{18} = N_{VP} + N_{\lambda 1} + N_{\lambda 2} = N_{VP} + \left((C_{OT} - C_O) \left\{ \left[\lambda_1 e^{\frac{-\alpha}{\lambda_1} + b_1} (1 - e^{-4}) \right] + \left[\lambda_2 e^{\frac{-\alpha - 4\lambda_1}{\lambda_2} + b_2} \right] \right\} \right) + \lambda_1 C_O (Z - 1) \quad \text{(S9)}.$$

2. Supporting Figures

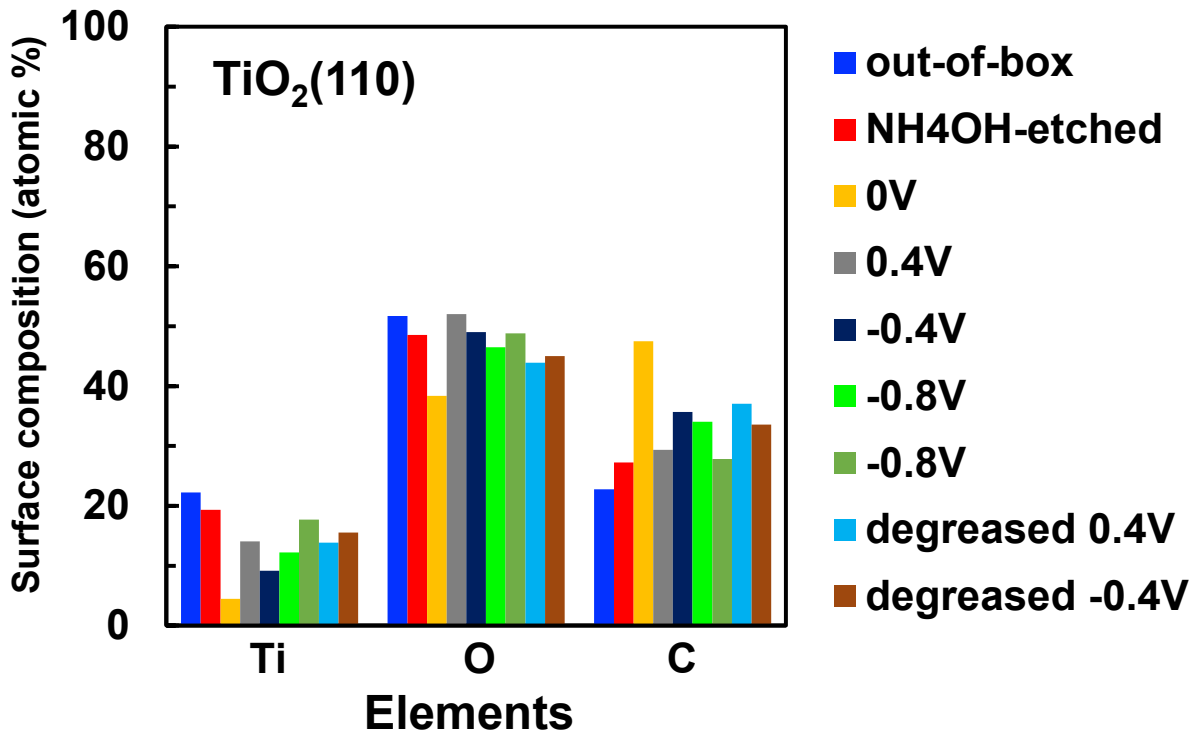

Figure S1. Surface composition measured by XPS for elements visible in the spectra. Most spectra were measured after diffusion on specimens diffused with applied bias; several values of applied bias V_{appl} (vs Ag/AgCl) are represented. Diffusion temperature was 70°C in all cases. "Degreased" means surface preparation included only the degreasing step, not etching by NH_4OH. Two specimens were measured before submersion; "out-of-box" and "NH4OH-etched" respectively mean XPS was performed on the specimen before any surface conditioning and after etching by NH_4OH. The elemental composition exhibits no clear relationship with either surface preparation or V_{appl}.

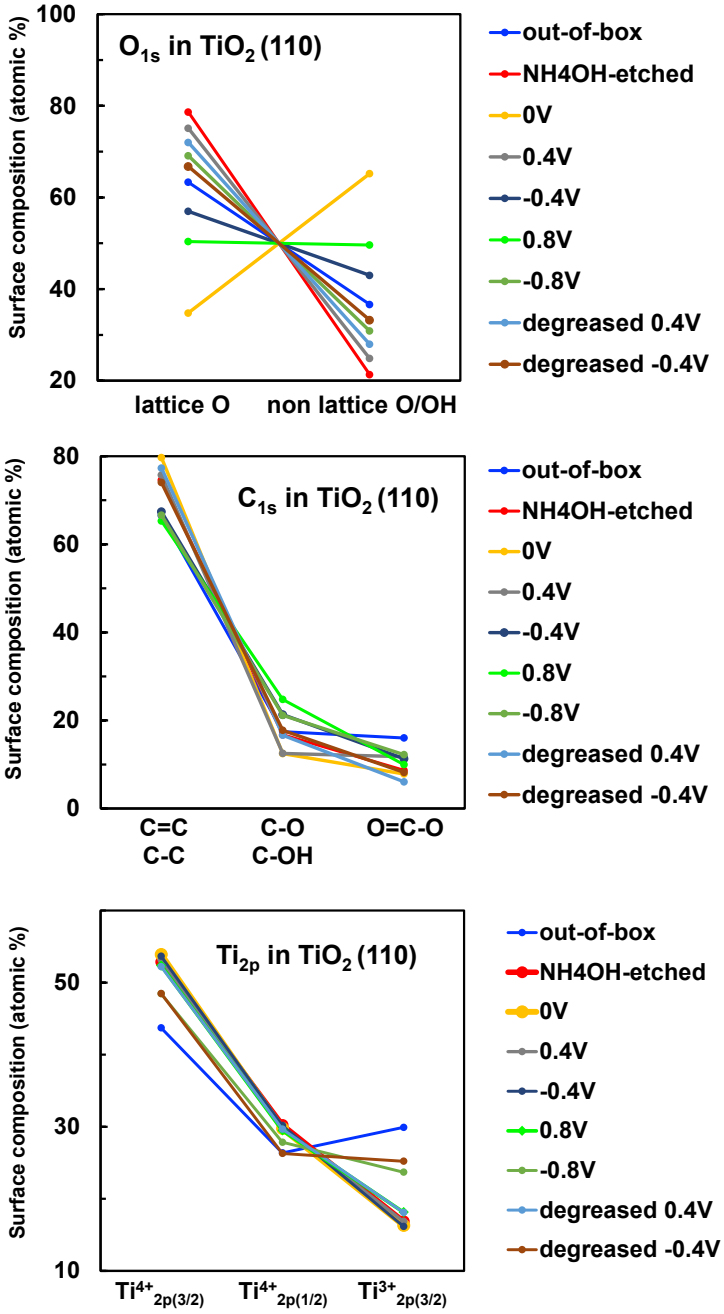

Figure S2. Chemical state information measured by XPS for elements visible in the spectra: (a) C, (b) O and (c) Ti. Most spectra were measured on specimens diffused with applied bias; several values of applied bias V_{appl} (vs Ag/AgCl) are represented. Diffusion temperature was 70°C in all cases. "Degreased" means surface preparation included only the degreasing step, not etching by NH_4OH. Two specimens were measured before submersion; "as-received" and "etched" respectively mean XPS was performed on the specimen before any surface conditioning and after etching by NH_4OH. The elemental composition exhibits no clear relationship with surface preparation or V_{appl}.

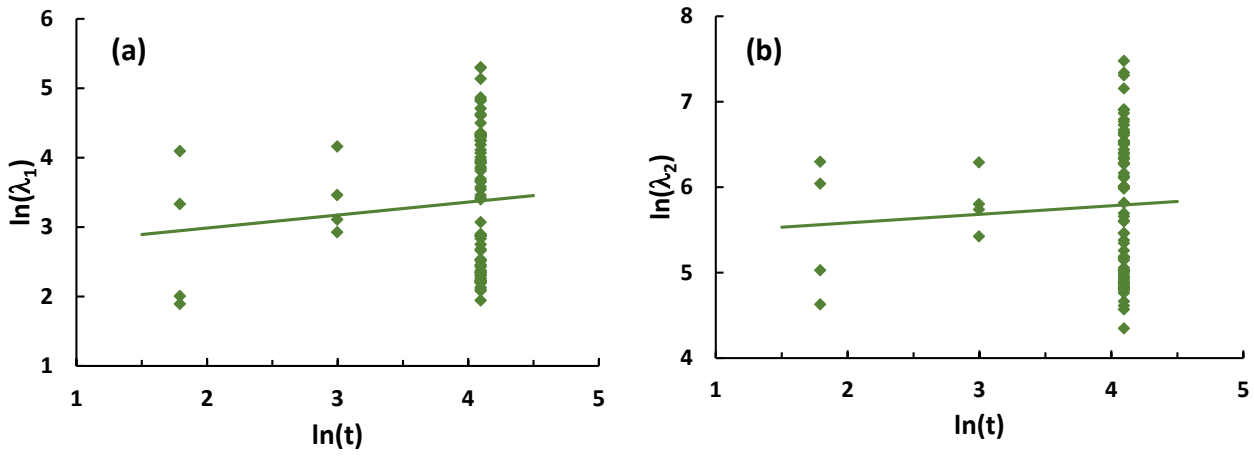

Figure S3. Profile metrics vs diffusion time *t* (min) with applied bias at 70°C for (a) λ_1 and (b) λ_2. Lines represent linear least squares fits. There is little variation of either λ_1 or λ_2 with t.

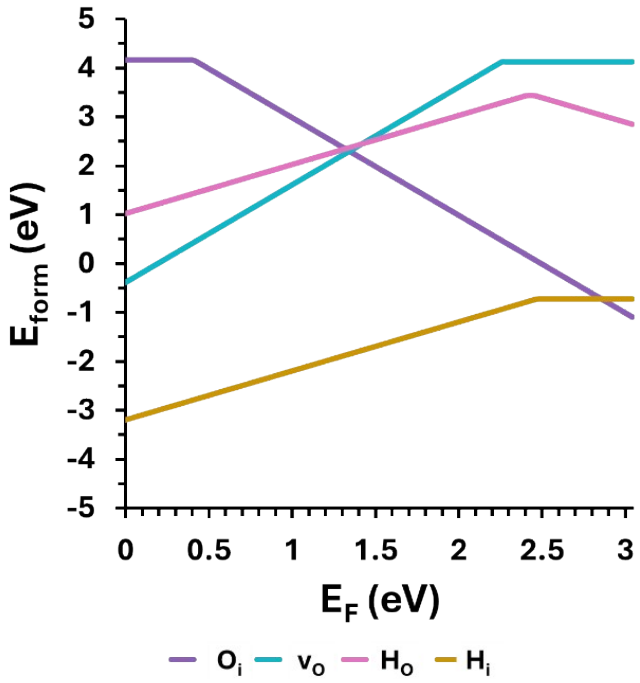

Figure S4. Formation energies vs E_F of point defects in rutile TiO_2.

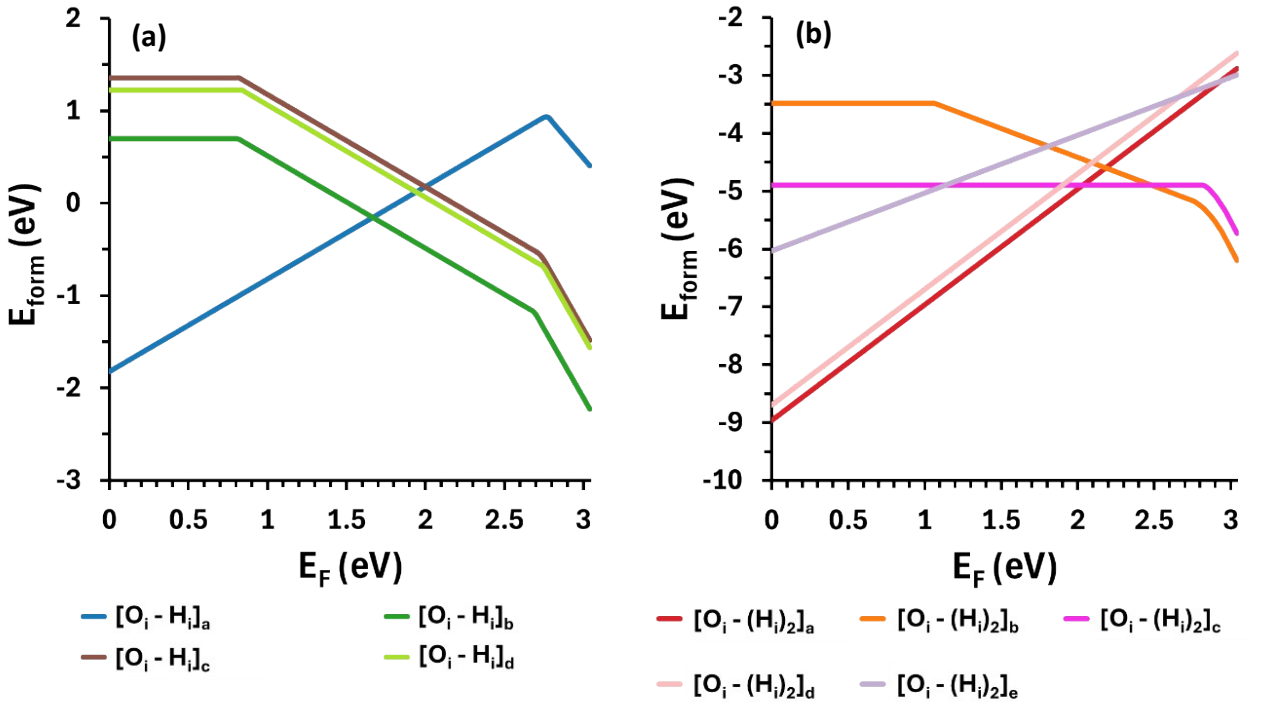

Figure S5. Formation energies of stable (a) O_i-H_i dimer O_i-$(H_i)_2$ and (b) trimer defect clusters in rutile TiO_2.

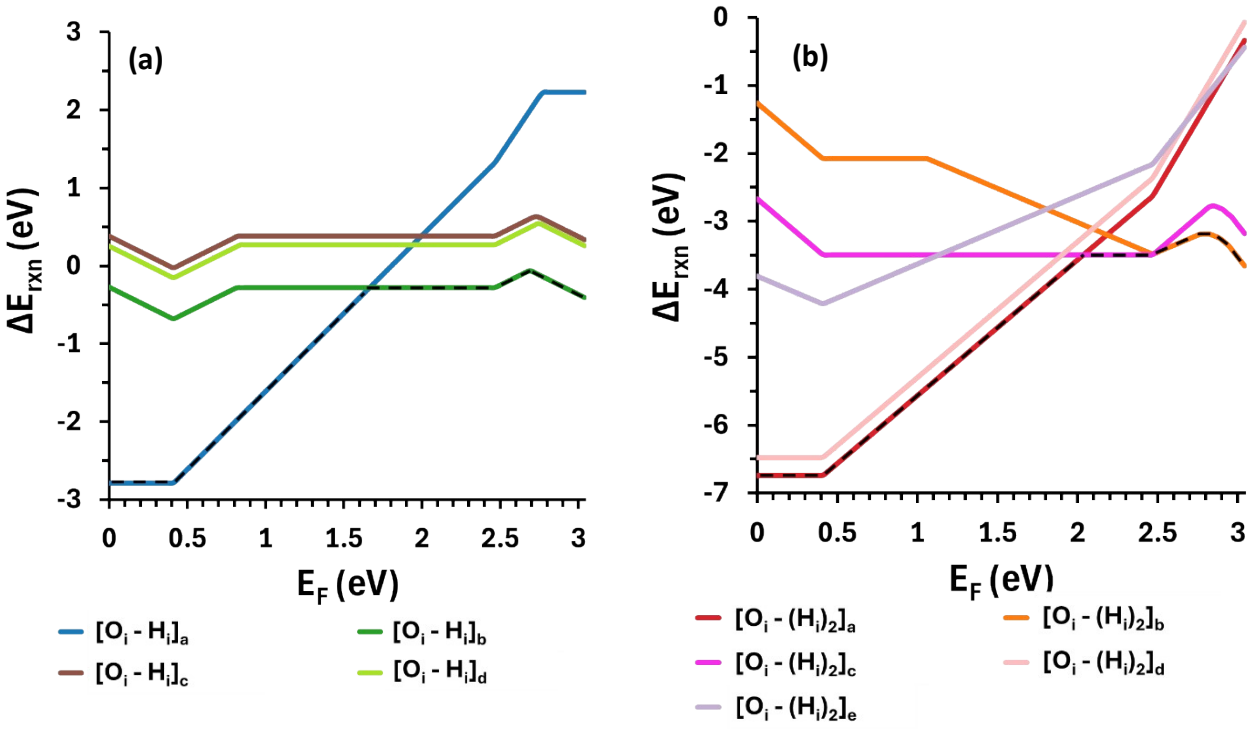

Figure S6. Reaction energies of (a) O_i-H_i dimer and (b) O_i-$(H_i)_2$ trimer clusters in rutile TiO_2. Identity of the most exothermic isomer varies with E_F and is traced with dashed lines.

3. Supporting Tables

Table T1. Atomic Force Microscopy parameters for surface treatments

Treatment	RMS Dev (nm)	Skew	Kurtosis
Degreased only	0.21	0.017	0.34
	0.23	0.059	0.36
	0.27	0.14	1.2
NH_4OH etched	0.058	-0.039	0.016
	0.10	0.21	-0.28
	0.18	0.33	-0.76
	0.23	0.094	1.12
	0.23	4.79	75.9
	0.23	5.32	85.9
	0.29	0.43	0.62

Table T2. Effective activation energies (eV) of profile metrics

Metric	Applied bias (dark)	Without bias (dark)	Without bias (UV)
F_{18}	0.39 ± 0.06	0.33 ± 0.05	0.13 ± 0.04
λ_1	0.05 ± 0.06	0.14 ± 0.05	0.061 ± 0.037
λ_2	0.21 ± 0.05	0.27 ± 0.05	-0.013 ± 0.025

Table T3. Profile metrics with applied bias at 70 °C.

	Mean (dark)	Mean (UV)
F_{18} (cm^{-2}s^{-1})	$(3.2 \pm 3.1) \times 10^{11}$	$(3.7 \pm 1.9) \times 10^{11}$
λ_1 (nm)	46 ± 45	59 ± 33
λ_2 (nm)	450 ± 370	630 ± 220

4. References

1 H. Jeong, I. I. Suni, R. Chen, M. Miletic, X. Su and E. G. Seebauer, Reactions of fluid and lattice oxygen mediated by interstitial atoms at the TiO2(110)–water interface, *Physical Chemistry Chemical Physics*, 2025, **27**, 9522–9536.

2 H. Jeong and E. G. Seebauer, Effects of Ultraviolet Illumination on Oxygen Interstitial Injection from TiO2 under Liquid Water, *The Journal of Physical Chemistry C*, 2022, **126**, 20800–20806.